https://doi.org/10.1016/j.nanoen.2020.105318

General Synthesis of Large-area Flexible Bi-atomic Subnano Thin Lanthanide Oxide Nanoscrolls

Miaomiao Wu[1], Tong Wu[2], Mingzi Sun[2], Lu Lu[2], Na Li[1], Chao Zhang[1], Bolong Huang,[2]* Yaping Du,[1]* and Chun-Hua Yan[1,3,4]

[1]*Key Laboratory of Advanced Energy Materials Chemistry, School of Materials Science and Engineering & National Institute for Advanced Materials, Centre for Rare Earth and Inorganic Functional Materials, Nankai University, Tianjin, 300350 P.R. China.*
[2]*Department of Applied Biology and Chemical Technology, The Hong Kong Polytechnic University, Hung Hom, Kowloon, Hong Kong SAR, 999077 P.R. China.*
[3]*Beijing National Laboratory for Molecular Sciences, State Key Laboratory of Rare Earth Materials Chemistry and Applications, PKU-HKU Joint Laboratory in Rare Earth Materials and Bioinorganic Chemistry, College of Chemistry and Molecular Engineering, Peking University, Beijing 100871, P.R. China.*
[4]*College of Chemistry and Chemical Engineering, Lanzhou University, Lanzhou 730000, P.R. China*

E-mail: bhuang@polyu.edu.hk (B.H.); ypdu@nankai.edu.cn (Y. D.)

Abstract

The surface ripple or scrolling phenomenon has been noticed in the synthesis of many ultrathin nanomaterials. However, the precise synthesis and control such subtle nanostructures are still highly challenging, indicating the untapped potential in the future nano energy systems. In this work, a simple but robust colloidal chemistry method is established to synthesize the ultrathin lanthanide oxide nanoscrolls, which achieves the atomically-thin thickness with scrolled edges for the first time. Detailed mechanism studies confirm that the scrolling behavior of nanoscrolls is initiated by surface charge perturbance induced by the adsorption of bromoalkyl group in the surfactant 3-bromopropyl trimethylammonium bromide. More importantly, the experiments demonstrate the reversible and controllable scrolling of the subnano thin lanthanide nanoscrolls. As proof of the actual application, the ultrathin lanthanide oxide nanoscroll/carbon nanotube film has been employed for the lithium-sulfur battery as the interlayer, which demonstrated excellent electrochemical performances. Our method is broadly applicable for the high-yield production of novel inorganic ultrathin nanostructures with great promise for applications in energy systems.

Keywords: Rare earth, Lanthanide oxides, Ultrathin nanostructure, Density functional theory, Lithium-sulfur battery

Introduction

Owing to the unique 4f electronic configurations, lanthanide elements are playing a pivotal role in both science and technology research progress for a wide range of applications[1-5] including the fields of luminescence, catalysis, magnetism[6,7] and electronics[8]. The research on the fabrications of low-dimensional nanosized lanthanide structures, such as nanotubes[9-14], nanosheets[15-18], nanowires[19,20] and nanoscrolls, have experienced rapid developments in the past decades. Particularly, the ultrathin nanoscrolls (NSs) attract intense research attention due to their unique properties from the bulk materials, originating from their remarkably small dimensions[21] and surface effects[22]. More importantly, monodisperse lanthanide nanoscrolls have not been reported so far. Since the intrinsic crystal structure of some lanthanide compounds is non-layered[23], the synthesis of atomically-thin lanthanide nanoscrolls by the simple exfoliation of bulk materials or by intercalation-swelling processes has been a significant challenge. Up to now, the mechanism of the scrolling becomes the focus of lots of research since it is able to supply significant references and guidance in the prediction, design, and synthesis of nanomaterials. For example, the scrolling in carbon[24] is due to induced-strain after separated from bulk materials; for N-rGOx sheets[25], scrolling can be achieved by strong magnetic adsorption of γ-Fe_2O_3; for indium sulfide[26], self-coiling is initiated by the weak interactions between ultrathin nanostructure embryo and building blocks. However, limited research works are focusing on the formation of surfactant-induced scrolling of ultrathin lanthanide oxides and the underlying mechanism.

The applications of the unique oxide materials have attracted intensive attention due to their applications in energy storage and conversion systems [27-30]. In particular, many works have reported the strong chemical interaction between the polar metal oxide materials and polysulfides, which is able to improve the performance of Li-S batteries, especially on the shuttle effect [31-34]. Such performance is attributed to their intrinsic polarity to realize the absorption of the polar polysulfides and the further suppression of the notorious shuttle effect. More importantly, the polar metal oxides are utilized as additive materials and host materials in the Li-S batteries, which both positively contribute to the electrochemical performances regarding both the polysulfide trapping and intermediates transformation acceleration. Compared to the normal two-dimensional nanosheet, the nanoscroll materials are able to display multiply interfaces, which supply more rapid electronic transportation channels, anion storage space [35-38]. Moreover, the nanoscroll has a higher tolerance for the volume expansion, which is significantly important for electrode materials during the charge/discharge cycles of batteries. Therefore, investigating the formation mechanism of lanthanide oxide nanoscroll will beneficial the application of other metal oxide nanoscrolls in the energy storage and conversion system in the future.

Herein, for the first time, we present the general colloidal chemistry method for the synthesis of ultrathin monodisperse single-crystalline lanthanide oxide NSs with only two atomic layer thickness. The formation mechanism of NSs provides a new strategy of manipulating the morphology of lanthanide oxide nanostructures by choosing appropriate surfactants. The uniform NSs were obtained in high yields with 3-bromopropyl trimethylammonium bromide (BPTAB) as the surfactant. Moreover, the scrolling behavior is reversible, in which the NSs change to flat nanosheets after the removal of the bromoalkyl-containing surfactant. The scrolling behavior is ascribed to the adsorption of bromoalkyl group in BPTAB, which leads to the uneven forces on the two sides of lanthanide oxide nanosheets. Efficient control over the transformation (as high as 100%) from Gd_2O_3 nanosheets into NSs is achieved by adding bromoalkyl-containing surfactant during the reaction process. Detailed theoretical calculations have been applied in both adsorption energies, dynamic simulations, formation energies and

electronic structures to reveal the underlying mechanism of NSs formation. More importantly, the actual application of such a conceptual advance is realized. In the lithium-sulfur (Li-S) battery, the as-synthesized NSs serves as the interlayer with excellent adsorption capability for polysulfides, which showed a promising capacity up to 945 mAh g^{-1} at the current density of 0.5 C with stable cycling performance.

Results and Discussion

The as-prepared Gd_2O_3 and Sm_2O_3 NSs were characterized by TEM and high-angle annular dark-field scanning TEM (HAADF-STEM). **Figure 1** shows that the high yield and uniform morphologies of Gd_2O_3 and Sm_2O_3 NSs (**Figure 1a-1c** for Gd_2O_3 and **Figure 1d-1f** for Sm_2O_3 NSs). The scale of square-like Gd_2O_3 NS has been determined with both diameter and length near 190 nm, where the ultrathin nanosheet center and scrolling edges are noted (**Figure 1a**). The average length of the scrolling edge is 30 nm, as shown in the HAADF-STEM image (**Figure S1**), the thickness of each layer is 0.74 nm. **Figure 1b** clearly demonstrates that the scroll consists of four layers, each with a thickness of two atomic layers. The corresponding crystal structure model of cubic Gd_2O_3 shows that Gd atoms and O atoms are packed into a Gd-O two-atom-layer (4 × 4 × 4 supercells). Compared with the crystal lattice of the sheet-like part (**Figure S2**), the lattice of the scrolls exhibits some distortion (**Figure 1c**). The distance between the lattice fringes is 0.30 nm, corresponding to the (222) plane of Gd_2O_3. As for the circular Sm_2O_3 NSs, the diameter is ~190 nm with edges scrolled up on two sides (**Figure 1d**). **Figure 1e** is the magnified image of the area within the red box in **Figure S3**, which shows that the scroll consists of three layers, each with two atomic layers thickness. The corresponding crystal structure model of cubic Sm_2O_3 shows that Sm atoms and O atoms are packed into the Sm-O two-atom-layer (4 × 4 × 4 supercells). Similarly, the thickness of each layer is 0.74 nm. The lattice distortion is also identified in the scrolling edge of Sm_2O_3 NSs (**Figure 1f**) as compared to the sheet-like part (**Figure S4**). The distance between the lattice fringes is 0.30 nm, corresponding to the (222) plane of Sm_2O_3.

In order to identify the crystal structures of the NSs, X-ray diffraction (XRD) characterizations were carried out. As shown in **Figure S5**, both ultrathin Sm_2O_3 NSs (JCPDS: 74-1989) and Gd_2O_3 NSs (JCPDS: 43-1014) exhibit a cubic phase with lattice parameters of a = b = c = 7.252 Å and lattice parameters of a = b= c= 7.616 Å, respectively. Two different Gd_2O_3 morphologies (nanoscrolls and nanosheets) were further characterized by Raman spectroscopy (excitation at 532 nm). The spectra (**Figure 1g**) of NSs and nanosheets both have three major peaks. For Gd_2O_3 NSs, the highest peak is at 374 cm^{-1} (the Fg + Ag mode), corresponding to the cubic phase, which is in agreement with previous literature on ultrathin Gd_2O_3 nanostructure[34]. For Gd_2O_3 nanosheets, which are synthesized by hexadecyl trimethyl ammonium bromide (CTAB), the highest peak is at 385 cm^{-1}. The blueshift for the NSs with respect to nanosheets indicates the presence of lattice strain resulting from the scrolling behavior[35]. The electron energy loss spectroscopy (EELS) elemental mapping images of ultrathin Gd_2O_3 NSs are shown in **Figure 1h**, confirming the uniform distribution of oxygen and gadolinium over the entire NS structure. Similar results are also found for ultrathin Sm_2O_3 (**Figure 1i**). X-ray photoelectric spectroscopy (XPS) was also used to investigate Gd_2O_3 NSs and nanosheets. In Gd_2O_3 NSs, the Br/Gd molar ratio was found to be 21%; whereas in Gd_2O_3 nanosheets, the Br/Gd ratio was 8% (**Figure S6**), suggesting that the Br content on the surface of NSs is more than two times higher than the nanosheets. These results imply that the bromine-containing species on the surface is the primary cause of the scrolling.

Scrolling is a common and natural behavior for two-dimensional nanostructures such as boron nitride, niobate[39], graphene[40-42], titanate[43] as well as transition metal dichalcogenides

(TMDs)[44]. The special structures with unique properties have attracted broad attention to investigate the formation mechanism of NSs. Up to date, the origins of the scrolling behavior have been ascribed to the decrease of temperature (MoS_2 monolayer flakes)[45], surface adsorption of the organic molecules (VO_2)[46] and hydrogenation effect (graphene)[47]. However, the scrolling behavior of Gd_2O_3 NSs displays a distinct mechanism from the following aspects: (1) There are no alien nanoparticles (like magnetic Fe_3O_4 for N-rGOx) in the reaction system to induce the scrolling; (2) Our synthesis follows a colloidal oil strategy, which is quite different from the reaction conditions mentioned above. Meanwhile, the unchanged reaction conditions during the morphological evolution cannot induce the lattice strains. Therefore, the scrolling in our Gd_2O_3 NSs should originate from a different mechanism, in which the adsorption of bromoalkyl group plays a central role. The evolution process of the NSs is illustrated in **Figure 2a**. Initially, the mixed solvent comprising OM, OA and ODE interacts with $Gd(CH_3CO_2)_3$ and BPTAB. The thick blocks of stacking nanosheets are formed at 260 °C for 5 min (as shown in **Figure 2b**). After 20 min at 260 °C, the edges of the nanosheets in the stacked blocks become scrolled up (**Figure 2c**). As the reaction further proceeds, the NSs are exfoliated from the stacked blocks and dispersed into the solution (**Figure 2d**). Importantly, after removing the bromoalkyl-containing surfactant by a surface medication method, the NSs become flattened ultrathin nanosheets (**Figure 2e**). The representative stages during the entire evolution process of the NSs are characterized by TEM and summarized in **Figure S7**.

A series of control experiments have been carried out to further verify the role of bromoalkyl groups in this reaction system. The summarized of the experiments was in **Table S1**. We found that the obtained products have scrolled edges with bromoalkyl group (BPTAB **Figure 3a**) and (2-bromoethyl) trimethylammonium bromide (**Figure 3b**). However, the pure nanosheets were obtained without bromoalkyl group (**Figure 3c, d**). Although these surfactants in the comparison experiments all show similar bromide structures, where the presence of the bromoalkyl group dominates the main difference in the final morphologies of the structures. The bromoalky group shows strong polarization in the charge distribution due to the strong electronegativity of the Br terminal. Such a unique structure is able to perturb the local electronic structure of Gd_2O_3 and trigger the intrinsic instability to induces the scrolling behaviors. More interestingly, NSs were obtained when we used CTAB as the surfactant and deliberately introduced a series of bromoalkyl-containing organic reagents (1,5-dibromopentane, 1,6-dibromohexane, **Figure S8a, b**) into the reaction system at the beginning of the reaction. Meanwhile, the as-synthesized Gd_2O_3 nanosheets were obtained using CTAB (the entire reaction process was showed in **Figure S9**). However, when the BPTAB was added into the system after 15 min at 260 °C, a large number of NSs were observed at the end of the reaction (**Figure S10**). Therefore, the addition of the bromoalkyl group provides sufficient adsorption energy to drive the formation of NSs, which caused an imbalance in surface force. Consequently, the nanosheets became NSs exfoliated from the stacked blocks. With 1 mmol or 2 mmol bro-moalkane introduced, the ultrathin nanosheets were obtained. When the concentration of bro-moalkane increased to 4 mmol, the products took the form of thick NSs (**Figure S11**).

Moreover, we systematically synthesized a series of lanthanide oxides (Sm_2O_3, Gd_2O_3, Eu_2O_3, La_2O_3, Yb_2O_3) to compare their morphologies. By changing the reaction conditions, we found that Sm_2O_3 and Gd_2O_3 were obtained as NSs, whereas La_2O_3, Eu_2O_3 and Yb_2O_3 were in the form of nanosheets (**Figure S12**). To further understand the formation of NSs and verify our assumption on the adsorption energies, we have calculated the adsorption energies of BPTAB on the five different lanthanide oxides. To be consistent with the experimental characterization

of the exposed plane in the HAADF-STEM image, all the calculations are based on the (222) plane. The top row of **Figure S12** showed the models of the adsorption of bromoalkyl group on the surface of lanthanide oxides. Notably, the adsorption energies on Sm_2O_3 and Gd_2O_3 NSs are obviously lower than the other surface planes, which confirms the much stronger adsorption trend of bromoalkyl group.

In addition, we have investigated the scroll nanosheet of Gd_2O_3 based on both dynamic simulation and the density functional theory (DFT) calculations. For dynamic situations, we have simulated the Gd_2O_3 nanosheet with different scroll angles under 298 K to observe the scroll situations. For the pristine Gd_2O_3 nanosheet, the dynamic simulation still induces the distortion, which indicates the potential instability of Gd_2O_3 nanosheet as an intrinsic feature to form NS. Such NSs become more evident when we apply an initial scroll angle to the nanosheet. From the scroll angle 15° to 25°, the NS structure has been preserved after dynamic simulations (**Figure 4a**). Within the limited scroll angle, the pressure in the dynamic scroll first becomes higher and then becomes stable, which demonstrates the releasement of intrinsic pressure by the formation of NS to reach the relatively stable structure (**Figure 4b**). Moreover, the NS stabilizes the system with the decreasing energies, supporting a high preference for spontaneous NS. This demonstrates that the formation of Gd_2O_3 NS requires the initiation from dynamic environment changes such as the surfactant (**Figure 4c**).

Meanwhile, we also considered the DFT calculations under 0 K to compare with the dynamic simulations. As the NS angle becomes larger, we notice the change of the bonding and anti-bonding orbitals, especially near the scroll region. The couplings between orbitals become weak when the scroll angle reaches 60°. These results demonstrate the formation of NS also affects the electronic environment. Moreover, the structure relaxation shows the structure distortion rather than the natural NS structure in dynamic simulations, which is ascribed to the different relaxation environment (**Figure 4d**). We have a further look at the Gd sites near the scroll region regarding the projected partial density of states (PDOSs). For the Gd sites near the scroll edge, we notice the strong contribution from both 5d and 4f orbitals. The 5d orbitals cross the Fermi level (E_F). As the NS angle increases to 60°, the 4f bands show varied intensity while 5d orbitals split near the E_F. Among different surfactants, the stronger disturbance by the surface charge distribution from bromoalkyl group leads to the intrinsic instability with scrolling behaviors[48]. The strong interactions between the Gd_2O_3 and bromoalkyl group lead to the inhomogeneous charge distribution and further inevitably result in the anomalies electronic and scrolling behaviors (**Figure 4e**). From an energetic perspective, we observe a distinct trend with dynamic simulations. The formation of NS without any external trigger is more difficult as the distortion angle becomes larger. Especially for the scroll angle reaches 60°, the formation dramatically increases. In addition, the pressure change also shows a converse trend with the dynamic calculation, where the large pressure is induced by the distorted structure rather than the stabilized NS with released intrinsic pressure (**Figure 4f**).

Therefore, our preliminary results indicate that the spontaneous formation of NS requires external stimuli such as the surfactant to break the balance of original bonding and coupling stability to initiate the NS formation.

Considering the outstanding adsorption property of ultrathin nanomaterials and the scroll structure, we applied the lanthanide oxides NSs with carbon nanotube (CNT) as a separator for lithium-sulfur batteries to improve the stability of batteries. **Figure 5** illustrates the three different battery configurations in the controlled experiments. Configuration A is a Li-S cell with the pristine separator; Configuration B has a CNT interlayer; Configuration C has a CNT–

lanthanide oxides interlayer. The charge/discharge voltage profiles of the electrode with a sulfur content of 80 wt% and four different interlayers in the 1st, 10th, 50th, and 100th cycles are shown in **Figure 5a-d**. Two typical discharge plateaus are observed, corresponding to two electrochemical processes. The higher discharge voltage plateau (at 2.35 V) indicates the reduction of elemental S to Li_2S_8; the lower discharge voltage plateau (at 2.11 V) represents the conversion of polysulfides to Li_2S_2/Li_2S, which contributes to the main discharge capacity (≈80%) of a Li-S cell. As shown in **Figure 5a**, the pristine separator showed an initial discharge capacity of 310 mAh g^{-1} and 334 mAh g^{-1} at the 100th cycle. The cell with the CNT interlayer showed capacities of 834 mAh g^{-1} and 589 mAh g^{-1} at the 1st and 100th cycles, respectively (**Figure 5b**). Moreover, the cell with the Gd_2O_3-CNT interlayer (945 mAh g^{-1} at 1st cycle) (**Figure 5c**) and Sm_2O_3-CNT interlayer (905 mAh g^{-1} at 1st cycle) (**Figure 5d**) showed excellent electrochemical performances. The corresponding discharge capacity (Q_H) is often used to evaluate the polysulfide-trapping capabilities of cells[49,50]. The Q_H of the Gd_2O_3-CNT interlayer in the 100th cycle was 80% of that in the first cycle (the Q_H of Sm_2O_3-CNT interlayer in the 100th was 77% of that in the first cycle), indicating that the loss of active sulfur was greatly suppressed by the Gd_2O_3-CNT and Sm_2O_3-CNT interlayer. **Figure 5e** showed the cycle performances of the cells. at the same sulfur loading (80 wt%) and galvanostatic charge/discharge rate, i.e., 0.5 C (1 C = 1672 mA g^{-1}), the cycling stability of the Li–S cells was improved significantly by the stepwise introduction of a CNT film, Gd_2O_3-CNT interlayer and Sm_2O_3-CNT interlayer. The synergetic effects of the Gd_2O_3-CNT interlayer led to an initial discharge capacity of 951 mA h g^{-1}, and the retention after 100 cycles was ~81%. In contrast, the cell with the pristine separator showed a lower initial discharge capacity, with fast capacity degradation in 100th cycles. Electrodes with the Gd_2O_3-CNT interlayer gave excellent rate performances because of the synergetic effect of the structure. **Figure 5f** shows that the electrodes had discharge capacities of 945, 895 and 832 mA h g^{-1} at corresponding charge rates of 0.5, 1 and 2 C. The cell with Sm_2O_3-CNT interlayer showed the similarity of the Gd_2O_3-CNT interlayer. As shown in Figure 6g, the long-term cycling properties of the Gd_2O_3-CNT interlayer at 0.5 C for 500 cycles maintained a capacity of 498 mA h g^{-1}. Then, the capacity retention was 81% from 200th to 500th cycle. The cyclic voltammetry (CV) profiles of the electrode with the pristine separator and Gd_2O_3-CNT interlayer for the first 2 cycles are shown in **Figure 5h-i**. The cell with the pristine separator suffered from severe polysulfide shuttling, resulting in hysteresis of the redox peaks as large as 0.309 V. While in the cell with Gd_2O_3-CNT interlayer the hysteresis of the corresponding redox peaks was only 0.288 V, indicating little polarization of the electrode.

Conclusion

In this paper, we have established an efficient and simple colloidal chemistry approach to synthesize the lanthanide oxide NSs with atomic layer thickness. The underlying mechanism of the scrolling behavior has also been revealed by detailed investigations. Our study in both experimental characterizations and theoretical investigations demonstrates the formation of Gd_2O_3 and Sm_2O_3 NSs originate from the initiation by the additives containing bromoalkyl groups. Their uneven adsorptions on the nanosheets lead to the unbalanced surface force distribution and further result in the self-scrolling behavior. Meanwhile, the scrolling is reversible, the removal of the bromoalkyl group through surface modification enables complete unfold the NSs into the flat sheets. Moreover, the superior performances of these unique NSs are confirmed in the Li-S battery as the interlayer separator, which significantly improves the stability of batteries. This work has supplied valuable references for future functional rare earth related energy materials design, synthesis, and applications in broad fields.

Acknowledgements
We gratefully acknowledge the support from the China National Funds for Excellent Young Scientists (21522106), the Natural Science Foundation of China (21771156), and the Early Career Scheme (ECS) fund (Grant No.: PolyU 253026/16P) from the Research Grant Council (RGC) in Hong Kong. Electron microscopy work was performed at the Center for Functional Nanomaterials, Brookhaven National Laboratory, which is supported by the U.S. Department of Energy (DOE), Office of Basic Energy Science, under contract No. DE-SC0012704.

Competing Interests
The authors have declared that there is no competing interest.

References

[1] Ida, S.; Ogata, C.; Shiga, D.; Izawa, K.; Ikeue, K.; Matsumoto, Y. Dynamic Control of Photoluminescence for Self-assembled Nanosheet Films Intercalated with Lanthanide Ions by Using a Photoelectrochemical Reaction. *Angew. Chem., Int. Ed.* **2008**, *47*, 2480.

[2] Ran, J.; Zhu, B.; Qiao, S.-Z. Phosphorene Co-catalyst Advancing Highly Efficient Visible-Light Photocatalytic Hydrogen Production. *Angew. Chem., Int. Ed.* **2017**, *56*, 10373.

[3] Lingeshwar Reddy, K.; Balaji, R.; Kumar, A.; Krishnan, V. Lanthanide Doped Near Infrared Active Upconversion Nanophosphors: Fundamental Concepts, Synthesis Strategies, and Technological Applications. *Small* **2018**, *14*, 1801304.

[4] Wu, J.; Fujii, K.; Yashima, M.; Staykov, A.; Akbay, T.; Ishihara, T.; Kilner, J. A. A Systematic Evaluation of the Role of Lanthanide Elements in Functional Complex Oxides; Implications for Energy Conversion Devices. *J. Mater. Chem. A* **2018**, *6*, 11819.

[5] Zhou, J.; Leaño Jr., J. L.; Liu, Z.; Jin, D.; Wong, K.-L.; Liu, R.-S.; Bünzli, J.-C. G. Impact of Lanthanide Nanomaterials on Photonic Devices and Smart Applications. *Small* **2018**, *14*, 1801882.

[6] Long, J.; Lyubov, D. M.; Mahrova, T. V.; Cherkasov, A. V.; Fukin, G. K.; Guari, Y.; Larionova, J.; Trifonov, A. A. Synthesis, Structure and Magnetic Properties of Tris(pyrazolyl)methane Lanthanide Complexes: Effect of the Anion on the Slow Relaxation of Magnetization. *Dalton T.* **2018**, *47*, 5153.

[7] Wu, M.; Xue, Y.; Li, N.; Zhao, H.; Lei, B.; Wang, M.; Wang, J.; Luo, M.; Zhang, C.; Du, Y.; Yan, C. Tumor-Microenvironment-Induced Degradation of Ultrathin Gadolinium Oxide Nanoscrolls for Magnetic-Resonance-Imaging-Monitored, Activatable Cancer Chemotherapy. *Angew. Chem., Int. Ed.* **2019**, *131*, 6954.

[8] Zhao, H.; Xia, J.; Yin, D.; Luo, M.; Yan, C.; Du, Y. Rare Earth Incorporated Electrode Materials for Advanced Energy Storage. *Coordin. Chem. Rev.* **2019**, *390*, 32.

[9] Panchakarla, L. S.; Popovitz-Biro, R.; Houben, L.; Dunin-Borkowski, R. E.; Tenne, R. Lanthanide-Based Functional Misfit-Layered Nanotubes. *Angew. Chem., Int. Ed.* 2014, *53*, 6920.

[10] Macedo, A. G.; Ferreira, R. A. S.; Ananias, D.; Reis, M. S.; Amaral, V. S.; Carlos, L. D.; Rocha, J. Effects of Phonon Confinement on Anomalous Thermalization, Energy Transfer, and Upconversion in Ln^{3+}-Doped Gd_2O_3 Nanotubes. *Adv. Funct. Mater.* 2010, *20*, 624.

[11] Liu, L. Q.; Ma, E.; Li, R. F.; Liu, G. K.; Chen, X. Y. Effects of Phonon Confinement on the Luminescence Dynamics of Eu^{3+} in Gd_2O_3 Nanotubes. *Nanotechnology* **2007**, *18*.

[12] Yada, M.; Taniguchi, C.; Torikai, T.; Watari, T.; Furuta, S.; Katsuki, H. Hierarchical Two- and Three-Dimensional Microstructures Composed of Rare-Earth Compound Nanotubes. *Adv. Mater.* 2004, *16*, 1448.

[13] Wang, X.; Sun, X.-M.; Yu, D.; Zou, B.-S.; Li, Y. Rare Earth Compound Nanotubes. *Adv. Mater.* **2003**, *15*, 1442.

[14] Yada, M.; Mihara, M.; Mouri, S.; Kuroki, M.; Kijima, T. Rare Earth (Er, Tm, Yb, Lu) Oxide Nanotubes Templated by Dodecylsulfate Assemblies. *Adv. Mater.* 2002, *14*, 309.

[15] Zhang, L.; Kang, W.; Ma, Q.; Xie, Y.; Jia, Y.; Deng, N.; Zhang, Y.; Ju, J.; Cheng, B. Two-dimensional Acetate-based Light Lanthanide Fluoride Nanomaterials (F–Ln, Ln = La, Ce, Pr, and Nd): Morphology, Structure, Growth Mechanism, and Stability. *J. Am. Chem. Soc.* 2019, *141*, 13134.

[16] Zhang, Q.; Yan, B. Salt-Effect-Based Synthesis and Anomalous Magnetic Properties of Rare-Earth Oxide Nanosheets with Sub-1 nm Thickness. *Chem.-Eur. J.* **2012**, *18*, 5150.

[17] Mai, H.-X.; Zhang, Y.-W.; Sun, L.-D.; Yan, C.-H. Orderly Aligned and Highly Luminescent Monodisperse Rare-Earth Orthophosphate Nanocrystals Synthesized by a Limited Anion-Exchange Reaction. *Chem. Mater.* 2007, *19*, 4514.

[18] Zhao, F.; Yuan, M.; Zhang, W.; Gao, S. Monodisperse Lanthanide Oxysulfide Nanocrystals. *J. Am. Chem. Soc.* 2006, *128*, 11758.
[19] Zhang, Y.-W.; Yan, Z.-G.; You, L.-P.; Si, R.; Yan, C.-H. General Synthesis and Characterization of Monocrystalline Lanthanide Orthophosphate Nanowires. *Eur. J. Inorg. Chem.* 2003, *2003*, 4099.
[20] Wang, X.; Li, Y. Synthesis and Characterization of Lanthanide Hydroxide Single-Crystal Nanowires. *Angew. Chem., Int. Ed.* 2002, *41*, 4790.
[21] Hu, S.; Wang, X. Ultrathin Nanostructures: Smaller Size with New Phenomena. *Chem. Soc. Rev.* 2013, *42*, 5577.
[22] Du, Y. P.; Zhang, Y. W.; Yan, Z. G.; Sun, L. D.; Yan, C. H. Highly Luminescent Self-Organized Sub-2-nm EuOF Nanowires. *J. Am. Chem. Soc.* 2009, 131,16364
[23] Huo, Z.; Tsung, C.-K.; Huang, W.; Fardy, M.; Yan, R.; Zhang, X.; Li, Y.; Yang, P. Self-Organized Ultrathin Oxide Nanocrystals. *Nano Lett.* 2009, *9*, 1260.
[24] Wu, J.; Jiao, L.; Antaris, A.; Choi, C.; Xie, L.; Wu, Y.; Diao, S.; Chen, C.; Chen, Y.; Dai, H. Self-Assembly of Semiconducting Single-Walled Carbon Nanotubes into Dense, Aligned Rafts. *Small* **2013**, 9, 4142.
[25] Sharifi, T.; Gracia, E.; Barzegar, H.; Jia, X.; Nitze, F.; Hu, G.; Nordblad, P.; Tai, C.; Wagberg, T. Formation of Nitrogen-Doped Graphene Nanoscrolls by Adsorption of Magnetic γ-Fe_2O_3 Nanoparticles. *Nat. Commun.* 2013, *4*, 2319.
[26] Ni, B.; Liu, H.; Wang, P.; He, J.; Wang, X. General Synthesis of Inorganic Single-Walled Nanotubes. *Nat. Commun.* 2015, *6*, 8756.
[27] Li, J.; Luo, S.; Wang, C.; Tang, Q.;, Wang, Y.; Han, X.; Ran, Hao R.; Wan, J., Gu, X.;, Wang, X,; Hu, C. *Nano Research* 2020, *13*, 759.
[28] Wang, J.; Sun, X.; Xu, L.; Xia, J.; Yang, Y.; Yin, Z.; Luo, F.; Du, Y. Organic-Rare Earth Hybrid Anode with Superior Cyclability for Lithium Ion Battery, *Adv. Mater.Interfaces*, 2020, 7, 1902168.
[29] Xia, J.; Zhao, H.; Pang, W.; Yin, Z.; Zhou, B.; He, G.; Guo, Z.; Du, Y. Lanthanide doping induced electrochemical enhancement of $Na_2Ti_3O_7$ anode for sodium-ion battery, *Chem. Sci.* 2018, 9, 3421.
[30] Zeng, Z.; Xu, Y.; Zhang, Z.; Gao, Z.; Luo, M.; Yin, Z.; Zhang, C.; Xu, J.; Huang, B.; Luo, F.; Du, Y.; Yan, C.-H. Rare-earth-containing perovskite nanomaterials: design, synthesis, properties and applications, Chem. Soc. Rev. 2020, 49, 1109.
[31] Ji, X. L.; Evers, S.; Black, R.; Nazar, L. F.; Stabilizing lithium-sulphur cathodes using polysulphide reservoirs. *Nat. Commun.* 2011, *2*, 325.
[32] Seh, Z. W.; Li, W. Y.; Cha, J. J.; Zheng, G. Y.; Yang, Y.; Mcdowell, M. T.; Hsu, P. C.; Cui, Y. Sulphur-TiO_2 yolk–shell nanoarchitecture with internal void space for long-cycle lithium–sulphur batteries. *Nat. Commun.* 2013, *4*, 1331.
[33] Kim, J. W.; Augustyn, V.; Dunn, B.; The Effect of Crystallinity on the Rapid Pseudocapacitive Response of Nb_2O_5. *Adv. Energy Mater.* 2011, *2*, 141.
[34] Liang, X.; Hart, C.; Pang, Q.; Garsuch, A.; Weiss, T.; Nazar, L. F.; *Nat. Commun.* 2015, *6*, 5682.
[35] Mei, Y.; Solovev, A. A.; Sanchez, S.; Schmidt**,** O. G. Rolled-up nanotech on polymers: from basic perception to self-propelled catalytic microengines, *Chem. Soc. Rev.*, 2011, *40*, 2109-2119.
[36] Wang, L.; Yue, Q.; Pei, C.; Fan, H.; Dai, J.; Huang, X.; Li, H.; Huang W. Scrolling bilayer WS_2/MoS_2 heterostructures for high-performance photo-detection *Nano Research* 2020, *13*, 956-966
[37] Le Luyer, C.; García-Murillo, A.; Bernstein, E.; Mugnier, Wave-Guide Raman Spectroscopy of Sol–Gel Gd_2O_3 Thin Films. *J. Rare Earth* **2003**, *34*, 234..

[38] Rahman, M.; Davey, K.; Qiao, S.-Z. Advent of 2D Rhenium Disulfide (ReS_2): Fundamentals to Applications. *Adv. Funct. Mater.* **2017**, *27*, 1606129.
[39] Rahman, M.; Davey, K.; Qiao, S.-Z. Advent of 2D Rhenium Disulfide (ReS_2): Fundamentals to Applications. *Adv. Funct. Mater.* **2017**, *27*, 1606129.
[40] Cheng, Y.; Koh, L. D.; Wang, F.; Li, D.; Ji, B.; Yeo, J.; Guan, G.; Han, M. Y.; Zhang, Y. W. Carbon Nanoscroll–Silk Crystallite Hybrid Structures with Controllable Hydration and Mechanical Properties. *Nanoscale* **2017**, *9*, 9181.
[41] Zheng, J.; Liu, H.; Wu, B.; Guo, Y.; Wu, T.; Yu, G.; Liu, Y.; Zhu, D. Production of High-Quality Carbon Nanoscrolls with Microwave Spark Assistance in Liquid Nitrogen. *Adv. Mater.* 2011, *23*, 2460.
[42] Berman, D.; Deshmukh, S. A.; Sankaranarayanan, S. K. R. S.; Erdemir, A.; Sumant, A. V. Production of High-Quality Carbon Nanoscrolls with Microwave Spark Assistance in Liquid Nitrogen. *Science* 2015, *348*, 1118.
[43] Kobayashi, Y.; Hata, H.; Salama, M.; Mallouk, T. E. Scrolled Sheet Precursor Route to Niobium and Tantalum Oxide Nanotubes. *Nano Lett.* 2007, *7*, 2142.
[44] Fang, X.; Wei, P.; Wang, L.; Wang, X.; Chen, Bo.; He, Q.; Yue, Q.; Zhang, J.; Zhao, W.; Wang, J.; Lu, G.; Zhang, H.; Huang, W.; Huang, X.; Li, H. Transforming Monolayer Transition-Metal Dichalcogenide Nanosheets into One-Dimensional Nanoscrolls with High Photosensitivity. *ACS Appl. Mater. Interfaces* 2018, *15*, 13011.
[45] Cui, X.; Kong, Z.; Gao, E.; Huang, D.; Hao, Y.; Shen, H.; Di, C.-a.; Xu, Z.; Zheng, J.; Zhu, D. Rolling up Transition Metal Dichalcogenide Nanoscrolls via One Drop of Ethanol. *Nat. Commun.* 2018, *9*, 1301.
[46] Mai, L.; Wei, Q.; An, Q.; Tian, X.; Zhao, Y.; Xu, X.; Xu, L.; Chang, L.; Zhang, Q. Nanoscroll Buffered Hybrid Nanostructural VO2 (B) Cathodes for High-Rate and Long-Life Lithium Storage. *Adv. Mater.* 2013, *25*, 2969.
[47] Zhu, S.; Li, T. *J.* Hydrogenation Enabled Scrolling of Graphene. *Phys. D Appl. Phys.* **2013**, *46*, 075301.
[48] Sun, M.; Wu, T.; Huang, B.; *Nano Energy* 2020, *70*, 104484.
[49] Xiao, Z; Yang, Z; Wang, L; Nie, H; Zhong, M; Lai, Q; Xu, X; Zhang, L; Huang, S. A Lightweight TiO_2/Graphene Interlayer, Applied as a Highly Effective Polysulfide Absorbent for Fast, Long-Life Lithium–Sulfur Batteries. *Adv. Mater.* **2015**, 27, 2891.
[50] Su, YS; Fu, YZ; Guo, BK; Dai, S; Manthiram, A. Fast, Reversible Lithium Storage with a Sulfur/Long-Chain-Polysulfide Redox Couple. *Chem.-Eur. J.* **2013**, 19, 8621.

Figures

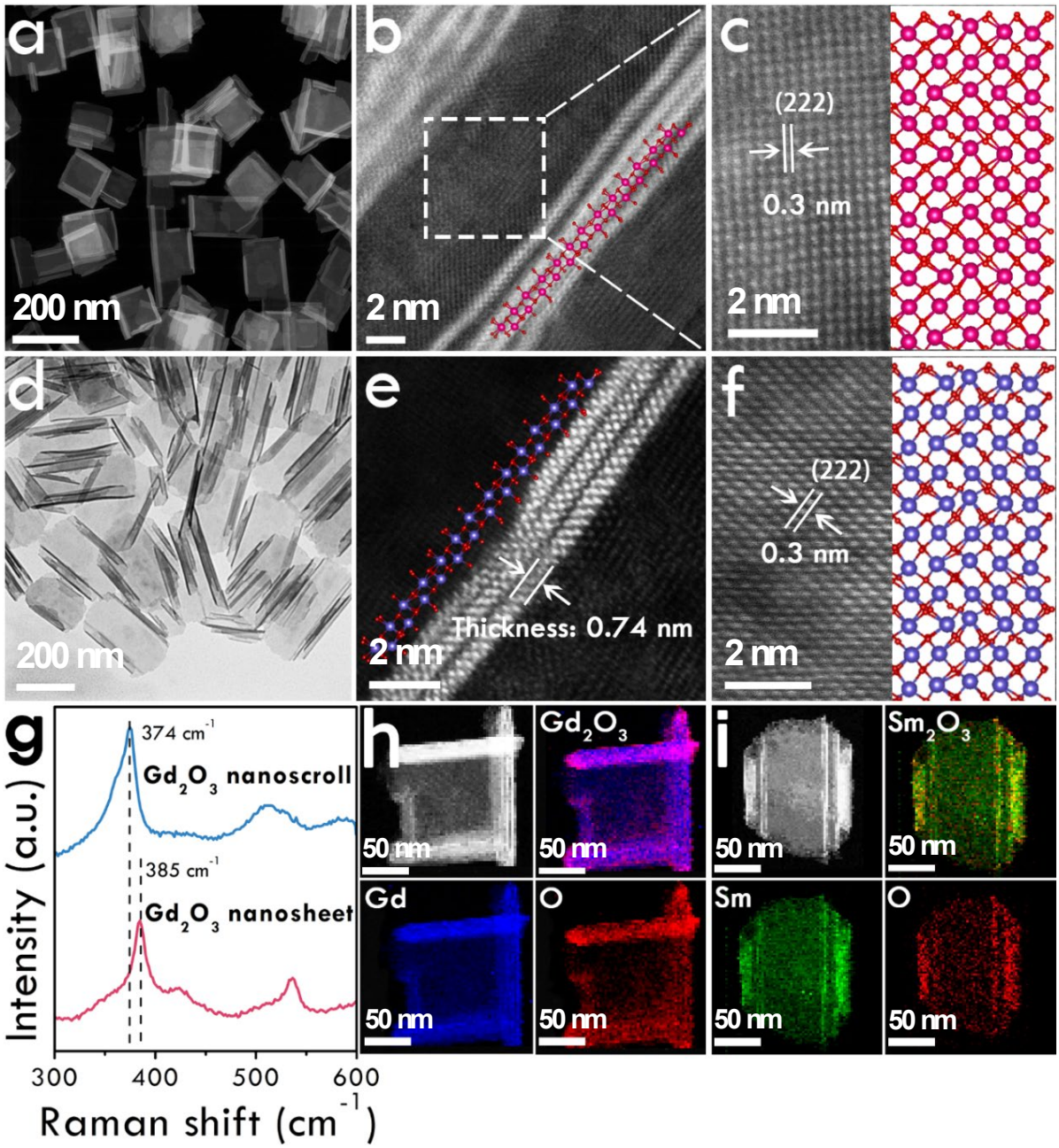

Figure 1. Characterizations of NSs. (a) TEM and (b, c) HAADF-STEM images of Gd_2O_3 NSs and the corresponding crystal structure model. (d) TEM and (e, f) HAADF-STEM images of Sm_2O_3 NSs and the corresponding crystal structure model. (g) Raman spectra of Gd_2O_3 NSs and nanosheets. (h) STEM image of Gd_2O_3 NSs and the corresponding EELS elemental mapping images of Gd_2O_3 and respective elements, Gd and O. (i) STEM image of Sm_2O_3 NSs and the corresponding EELS elemental mapping images of Sm_2O_3 and respective elements, Sm and O.

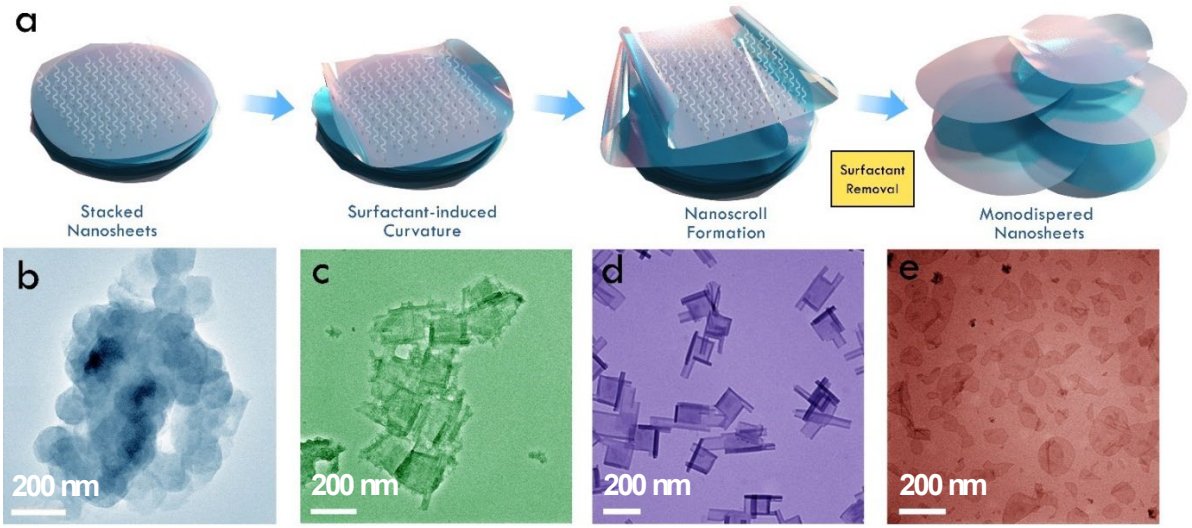

Figure 2. The formation mechanism and morphological evolution of Gd_2O_3 NSs. (a) Schematic illustration for the morphological evolution process. (b-e) TEM images demonstrating the four typical stages during the evolution: (b) sample extracted from the reaction mixture only 5 min after the mixture was heated to 260 °C, (c) sample extracted 20 min after 260 °C, (d) as-obtained Gd_2O_3 NSs (260 °C for 1 h) after the reaction, (e) ultrathin Gd_2O_3 nanosheets obtained after removal of the bromoalkyl-containing surfactant from Gd_2O_3 NSs.

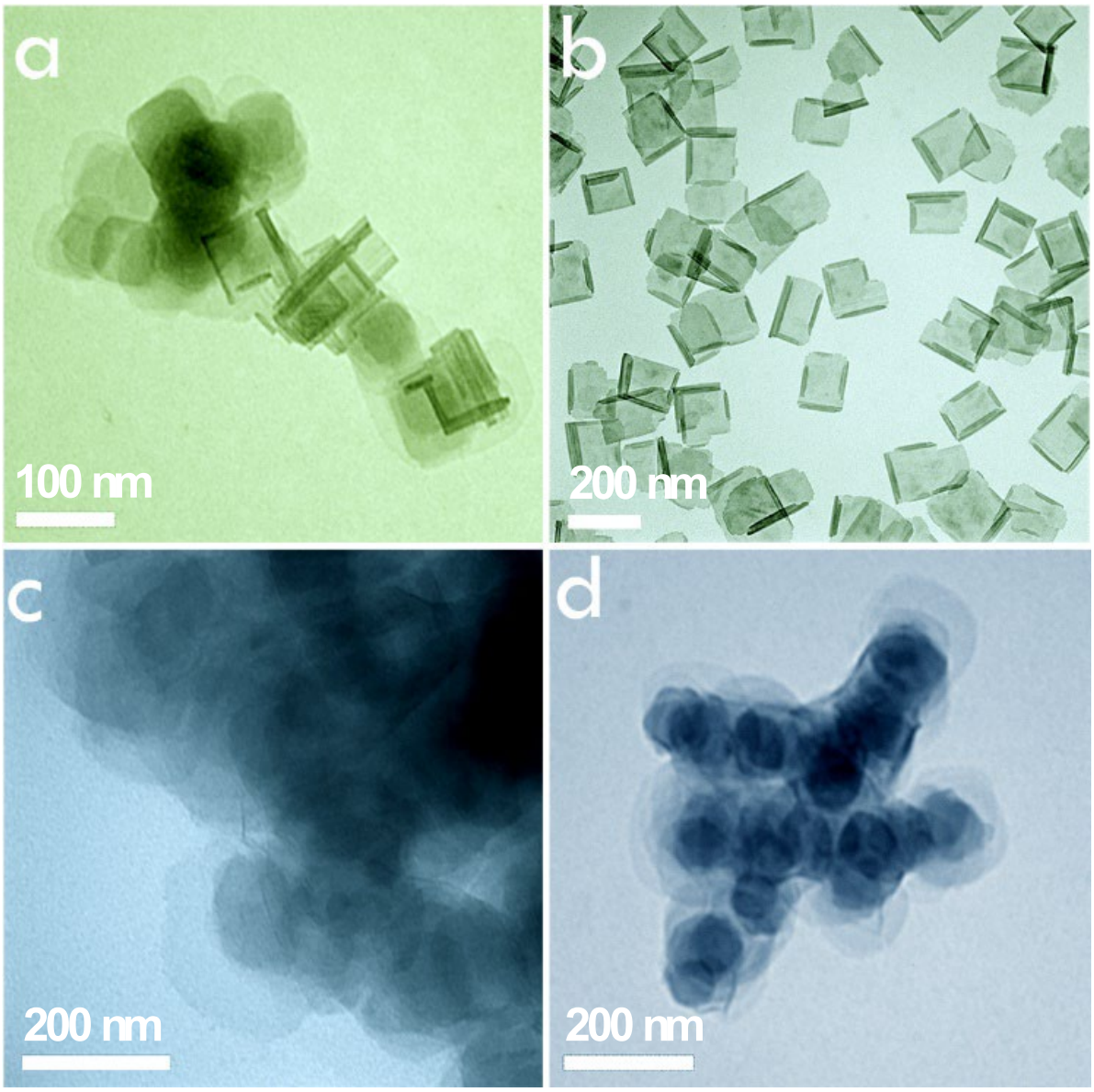

Figure 3. Gd_2O_3 with different morphologies obtained with different surfactants (a) Gd_2O_3 NSs obtained with (2-bromoethyl) trimethylammonium bromide. (b) Gd_2O_3 NSs obtained with BPTAB. (c) Gd_2O_3 nanosheets obtained with CTAB. (d) Gd_2O_3 nanosheets obtained with methyltrioctylammonium bromide.

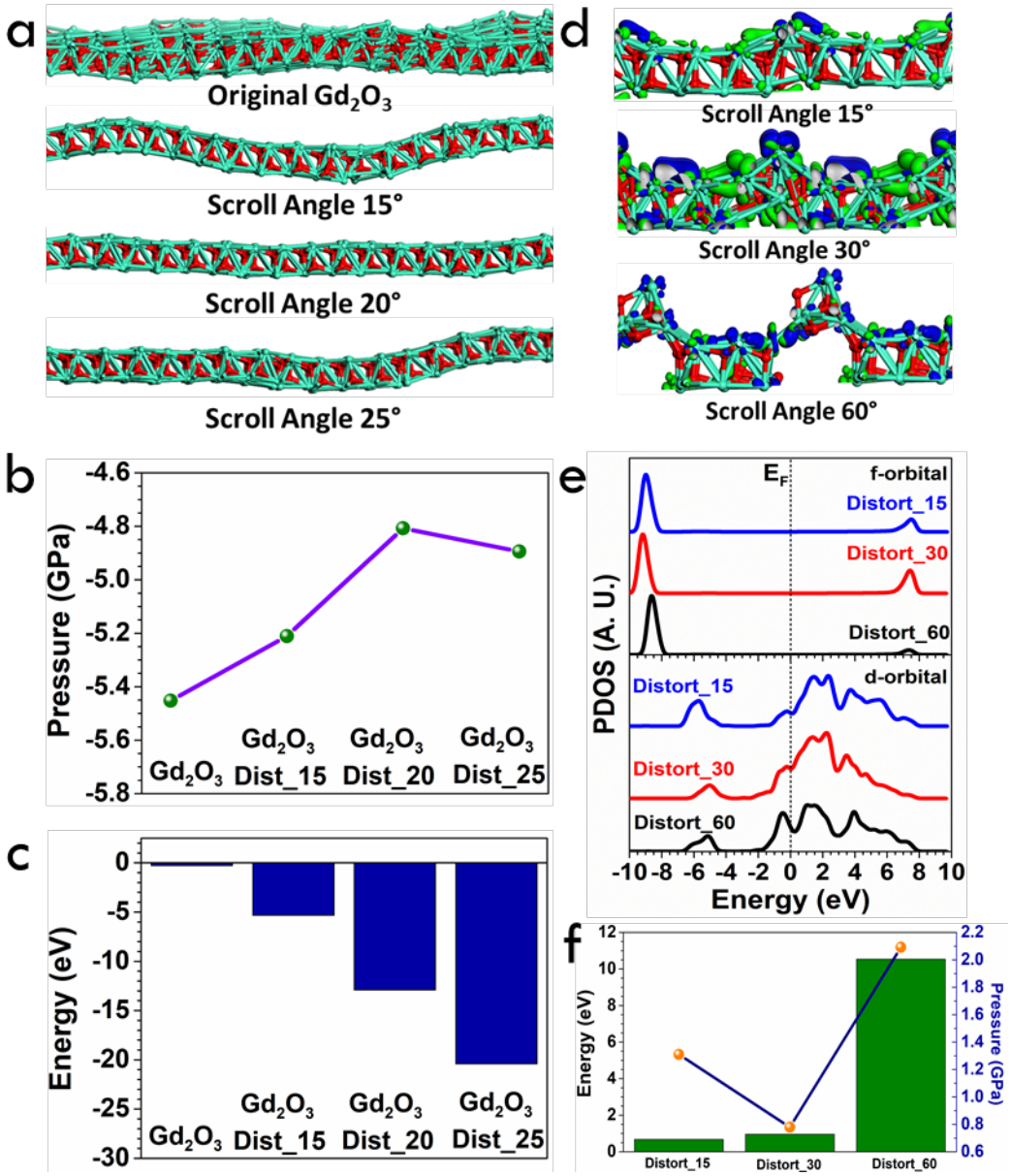

Figure 4. (a) Dynamic simulations of Gd_2O_3 NS. (b) The pressure changes of the Gd_2O_3 NS. Dist_15, Dist_20 and Dist_25 represent the distortion angle of 15°, 20° and 25°. (c) The energy changes of Gd_2O_3 NS. (d) Bonding and anti-bonding orbitals of Gd_2O_3 NS with different angles. (e) The PDOSs of the Gd sites at the scroll region. Distort_15, Distort_30 and Distort_60 represent the distortion angle of 15°, 30° and 60°. (f) The energy and pressure change of Gd_2O_3 NS.

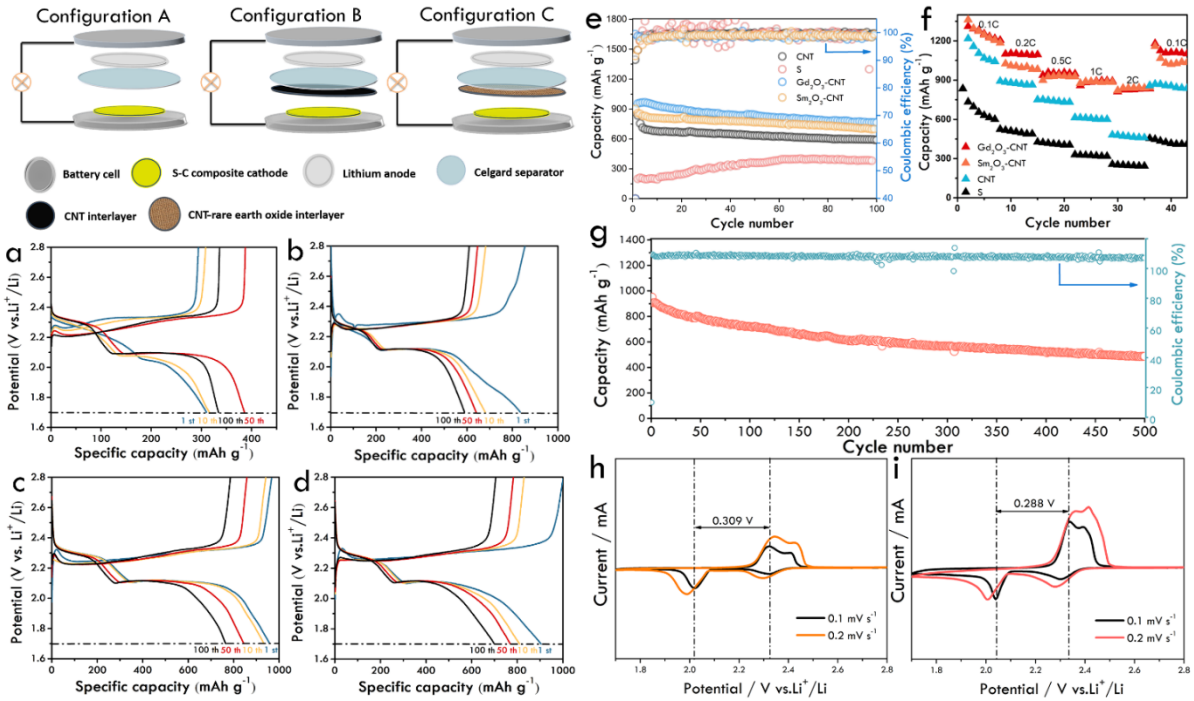

Figure 5. Illustrations of the three different battery configurations in the experiment and charge and discharge curves of the batteries with configurations of Celgard film as a separator (a) corresponding to Configuration A, carbon nanotube as a separator (b) corresponding to Configuration B, Gd_2O_3 NSs and carbon nanotube as a separator (c) and Sm_2O_3 NSs and carbon nanotube as a separator (d) corresponding to Configuration C. (e) cycling performance of the four different batteries. (f) rate capabilities of Li-S batteries with Celgard film, CNT, Gd_2O_3-CNT and Sm_2O_3-CNT interlayer. (g) long-term cycling properties at 0.5 C for 500 cycles with Gd_2O_3-CNT interlayer. The cyclic voltammetry profiles of the electrode with (h) pristine separator and (i) Gd_2O_3-CNT interlayer.